THE JOURNAL OF PHYSICAL CHEMISTRY C

Article

pubs.acs.org/JPCC

Flexible Self-Assembled Molecular Templates on Graphene

Kaustuv Banerjee,[†] Avijit Kumar,[†] Filippo Federici Canova,[‡] Shawulienu Kezilebieke,[†] Adam S. Foster,[‡,§] and Peter Liljeroth*[,†]

[†]Department of Applied Physics and [‡]COMP Centre of Excellence, Department of Applied Physics, Aalto University School of Science, 00076 Aalto, Finland

[§]Division of Electrical Engineering and Computer Science, Kanazawa University, Kanazawa 920-1192, Japan

Supporting Information

ABSTRACT: We report on molecular self-assembly employing a host−guest architecture to pattern the growth of molecules on graphene model surface. Under suitable conditions, the 1,3,5-benzenetribenzoic acid (BTB) self-assembles into an extended honeycomb mesh on graphene on Ir(111), with the molecules in the network being stabilized by linear hydrogen bonds between the carboxylic groups. The nanopores of the mesh are used to host and govern the assembly of cobalt phthalocyanine (CoPC) guest molecules. We characterize the assembled structures structurally and electronically using low-temperature scanning tunneling microscopy (STM) and density functional theory (DFT) calculations. At a coverage higher than one CoPc per pore, the flexible hydrogen bonds of the host network undergo stretching to accommodate two CoPCs in a single pore. When the pores are uniformly doubly occupied, the guest molecules arrange into a herringbone pattern. This minimizes the energy cost associated with the stretching and twisting of the hydrogen bonds between the BTB molecules. The phenomenon observed here can be used to tailor molecular assemblies on graphene to controllably modify its properties. In addition, it allows the formation of guest monomers and dimers stabilized mechanically on the surface of graphene, an archetypical weakly interacting substrate.

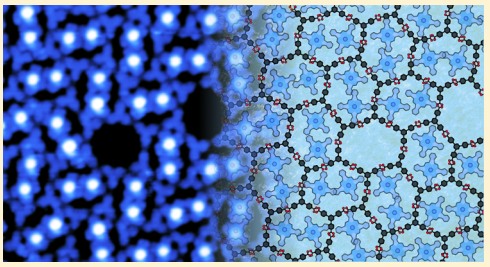

INTRODUCTION

Molecular self-assembly has been typically studied on metallic substrates and graphite, where the focus has been on understanding the basics of the assembly process on surfaces and to investigate in detail the structural properties of the formed assemblies.[1,2] Studies on graphene are much less advanced, and the work on controlled modification of its surface properties by molecular self-assembly is just starting.[3−5] It is expected that there are strong differences between molecular networks on graphene and metallic bulk substrates due to the weak, mostly van der Waals, molecule−substrate interactions on graphene.[6] However, the bulk material supporting graphene has a strong effect on its surface properties. The lattice mismatch between graphene and the substrate results in a periodic variation of the surface topography and electronic properties called the moiré pattern.[7,8] If graphene interacts strongly with the underlying substrate, as in the case of epitaxial graphene grown on ruthenium or rhodium crystals, the moiré is strongly corrugated. The local work function of the surface can also vary significantly within the moiré unit cell, which together with the topographic corrugation has a pronounced effect on the ordering of any molecular overlayer. On the other hand, when graphene is grown on silicon carbide, iridium, or platinum, the graphene−substrate interaction is much weaker and the corrugation and work-function difference across the periodic superstructure are also small. Thus, weakly coupled graphene e.g., G/SiC, G/Ir, is quite similar to free-standing graphene and a very clean model system to study self-assembly on weakly interacting substrates.[9]

In addition to forming an excellent model system to study molecular self-assembly, it has been argued that surface modification is an essential point in realizing the application potential of graphene and other 2D materials.[10−12] 2D materials consist only of surface atoms, and hence, it should be possible to strongly modify their properties by using adsorbed molecular layers. For example, adsorption of molecules can be used for charge doping depending on the relative alignment of the molecular orbitals and the graphene Fermi level.[13−15] In addition, it has been suggested that external periodic potential setup by a molecular layer could be used to tune the graphene band structure[16,17] in analogy with the effects due to the moiré pattern observed on graphene on h-BN devices.[18,19] On the other hand, sensor applications require tuning the graphene surface chemistry to boost selectivity and sensitivity,[20,21] and similar considerations also extend to catalysis on the graphene surface.[22]

On the simplest level, the molecular assembly on graphene is formed by close packing of molecules without intermolecular bonds, and the assembly is held together by weak van der Waals interactions. In more strongly interacting assemblies, one can utilize hydrogen, metal-coordination, or covalent bonds that

Received: February 17, 2016
Revised: April 5, 2016
Published: April 7, 2016

DOI: 10.1021/acs.jpcc.6b01638
J. Phys. Chem. C 2016, 120, 8772−8780

induce much stronger and directional interactions between the adsorbates.[23,24] Especially, hydrogen-bonded supramolecular assemblies based on a single (e.g., organic molecules with terminal carboxylic groups[25]) or multiple molecular components (e.g., PTCDI−melamine on metal[26] or epitaxial graphene[27]) offer an easy and predictable way to obtain two-dimensional nanoporous networks with hexagonal symmetry on a variety of surfaces. In this respect, single-step homomeric assemblies with the 3-fold symmetric tricarboxylic acids, trimesic acid (TMA), and benzene−tribenzoic acid (BTB) have been studied in detail on metal and graphite. Depending on the deposition conditions, both TMA and BTB have been observed to assemble into honeycomb networks with a period of ∼1.7 nm[28−32] and ∼3.2 nm,[33−37] respectively. Other phases, both porous and compact, have also been observed in conjunction with the honeycomb structure. So far, on graphene, only assembly of TMA at the solid−liquid interface has been studied. The obtained results were contrasting—while TMA was seen to assemble into a close-packed lattice on exfoliated graphene,[38] it was observed to form hexagonal porous network on graphene on copper foil.[39]

On a level of increased complexity, porous molecular networks can be used as templates for patterning the deposition of subsequent layers.[26,40−42] This would allow building up of multicomponent, hierarchical structures on surfaces. In particular, using periodic nanoporous arrays is an attractive way of templating molecular assembly on graphene with the intermolecular spacing and lattice symmetry of the guest molecules being tuned by the host network. In this work, we present low-temperature scanning tunneling microscopy (STM) and spectroscopy (STS) experiments complemented by density-functional theory (DFT) calculations on hydrogen-bonded honeycomb networks of 1,3,5-tris(4-carboxyphenyl)-benzene (BTB) with excellent long-range order on a graphene model system (epitaxial graphene on Ir(111), G/Ir(111)). In addition, we use these networks to pattern the assembly of cobalt phthalocyanine (CoPC) molecules. Hydrogen-bonded porous networks have been previously shown to host various metal phthalocyanine (MPC) molecules.[43] In these examples, the hydrogen-bonded network consisted of large and flexible molecular building units.[41,44] It was shown that depending on the ratio of the guest and the host molecules, the network could host MPC monomers or dimers by changing the network structure and adjusting the pore size. This flexibility was attributed to the distortion of the long alkyl chains and switching the position of the hydrogen bond.[45,46] In the present work, we demonstrate how slight deformations of the soft, hydrogen-bonded template can accommodate two guest molecules at higher loading of CoPC. Furthermore, the deformations of neighboring pores are correlated, which results in a formation of a herringbone pattern of the guest molecules. Using a simple toy model, this can be understood as arising from the minimization of the elastic energy stored in the hydrogen bonds of the template. This novel effect on soft templates on weakly interacting substrates is expected to be general, and it can be used to construct assembled structures that break the template symmetry.

METHODS

Experiments. All experiments were performed in ultrahigh vacuum (UHV) conditions with a base pressure of 1×10^{-10} mbar. The Ir(111) crystal was cleaned by repeated cycles of 2 kV Ne^+ sputtering, annealing in 5×10^{-7} mbar of oxygen at 1200 K, and flashing to 1600 K. Thereafter, graphene was grown on the Ir substrate by a combination of temperature-programmed growth (TPG) and chemical vapor deposition (CVD).[47] Initially, the substrate was exposed to 1×10^{-6} mbar of ethene (C_2H_2) for 30 s at room temperature and heated to 1600 K. Subsequently, with the temperature held at 1600 K, the substrate was exposed to 1×10^{-7} mbar of C_2H_2 for a further 30 s, after which the temperature was slowly brought down to room temperature. All molecules, viz. BTB, TMA, and CoPC, were bought from Sigma-Aldrich and used as is. BTB was evaporated onto the G/Ir sample kept at room temperature from a home-built thermal evaporator kept at a temperature of 500 K. The sample was subsequently annealed for an hour each, at 340 and 373 K. Well-ordered BTB network was observed only after the second annealing step. TMA was deposited at 415 K onto the G/Ir sample kept at room temperature; the sample was subsequently heated at 373 K for an hour. Evaporation of CoPC was done at 653 K from a Knudsen cell. Prior to CoPC deposition, a BTB/G/Ir sample was annealed at 373 K for an hour to get extended BTB network. Deposition of CoPC was done with the sample being held at room temperature; no further annealing was done to the sample after the deposition.

The STM experiments were done with a Createc LT-STM at $T = 5$ K. All images were taken with a cut Pt−Ir tip in the constant current mode. The spectra were taken with standard lock-in technique employing a SRS 830 lock-in amplifier with a small sinusoidal voltage of 50 mV peak-to-peak amplitude at 484.4 Hz. Some of the dI/dV spectra were taken in the constant current mode. The lock-in frequency is much higher than the bandwidth of the feedback circuit; i.e., the feedback should not respond to the small ac bias modulation. The STM images were processed with Gwyddion.[48]

Computations. All first-principles calculations in this work were performed using the periodic plane-wave basis VASP code[49,50] implementing the spin-polarized DFT. To accurately include van der Waals interactions in this system, we used the optB86P functional.[51,52] Projected augmented wave (PAW) potentials were used to describe the core electrons.[53] A kinetic energy cutoff of 450 eV (with PREC = accurate) was found to converge the total energy of all the systems to within 10 meV. All STM simulations were done using the basic Tersoff−Hamann approach.[54] The properties of bulk graphite and graphene, and available molecular information, were carefully checked within this methodology, and excellent agreement was achieved with experiments. Systematic k-point convergence was checked for all systems, and all atomic forces were relaxed until less than 0.02 eV/Å. For calculations of the full BTB molecular layer on graphene (in simulations the metallic substrate was ignored for simplicity), first the geometry of a pair of relaxed molecules, H-bonded together on the surface, were used to construct a unit cell. To match this with the underlying graphene unit cell, the graphene lattice constant was expanded by about 6%. To check that this made no significant differences to the interaction with BTB molecules, we compared adsorption energies for both the ideal and expanded graphene layer, and the difference was about 0.1 eV (less than 4% error). The distorted pore system was modeled by gradually increasing the lattice constant in one dimension (and correspondingly reducing it in the orthogonal direction) until it matched the average experimental distortion (about 5%).

In order to simulate the distortion pattern of the hexagonal BTB lattice in the presence of CoPC, we built a simple toy

DOI: 10.1021/acs.jpcc.6b01638
J. Phys. Chem. C 2016, 120, 8772−8780

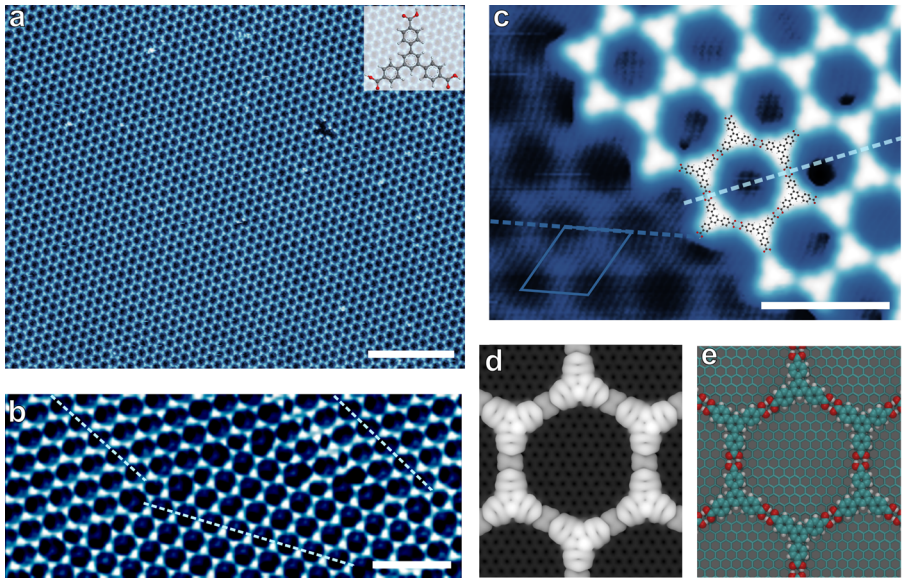

Figure 1. BTB self-assembly on epitaxial graphene on Ir(111). (a) Large-scale STM image of the BTB network. Inset shows the structure of BTB. Set-point parameters 1.59 V/5.7 pA. Scale bar 25 nm. (b) Misaligned and misoriented domains of the BTB hexagonal network on the same G/Ir(111) terrace. The lines indicate the "zigzag" direction of the BTB domains. Set-point parameters 1.68 V/8.1 pA. Scale bar 10 nm. (c) Zoomed-in STM image of an edge of a BTB network demonstrating that the BTB network is not aligned along a high-symmetry direction of the graphene moiré pattern (moiré unit cell indicated by the blue parallelogram). Set-point parameters −1.45 V/20 pA. Scale bar 5 nm. (d) Simulated constant-current STM image of the network at a bias of −1.5 V (see Methods section for the computational details). (e) Atomistic model of BTB network on graphene predicted in the simulations.

model of the system. All molecules are represented by two-dimensional rigid bodies, able to move in the simulation plane, and rotate around the plane normal. The mass of BTB is located on three circles, placed in the triangular pattern corresponding to the phenyl-COOH arms of the molecule. Similarly, CoPC is modeled as a single circular body, covering the whole area of the molecule. The scheme is shown in Figure S6 of the Supporting Information, where the circles are rigid colliders, preventing their mutual overlap. Additionally, neighboring BTB in the hexagonal lattice are connected by two harmonic springs that mimic the H-bonds between their −COOH terminations, which enforce both the correct positioning and alignment of BTB. The potential energy of the system is given by the total elastic energy stored in the bonding springs. A Langevin thermostat was applied to all rigid bodies, enabling temperature control. Since the mass, size, and interactions between molecules are somewhat arbitrary, this model will not accurately reproduce the dynamics of the system in general. However, in the regime of small distortions and low temperature, where the harmonic approximation is valid, the stretching modes of the BTB lattice should be described correctly. The simulations were performed with Unity 5 (http://unity3d.com) which implements rigid body dynamics integration and collision solver algorithms. The model's source code is freely available (https://github.com/fullmetalfelix/Simpleton) and simulated interactively in most Web browsers (http://fullmetalfelix.github.io/Simpleton).

RESULTS AND DISCUSSION

An overview of the self-assembled structure formed after deposition of 0.2 ML BTB on the G/Ir(111) substrate and heating the sample to 373 K for 1 h is shown in Figure 1a. The molecules assemble into an extended honeycomb network with a pore size of ∼2.5 nm, a pore-to-pore distance of ∼3.2 nm, and a molecular packing density of 0.18 molecule/nm^2. These observations are close to the literature reports on the self-assembly of BTB into a chicken-wire structure, either by UHV deposition on Ag(111)[33] or at solid−liquid interface on graphite.[34−37] Under the growth condition, the network covered major portions of the G/Ir(111) surface with large domains extending for hundreds of nanometers (Figure 1a). These domains extend seamlessly over step edges of the underlying iridium single crystal and wrinkles on the epitaxial graphene surface (Figure S1). In some cases, two or more domains of the hexagonal network, either laterally displaced or rotated with respect to each other, are observed on the same G/Ir(111) terrace (Figure 1b). The different BTB domains on the same terrace (i.e., with a single graphene orientation) have a broad distribution of different angles (a histogram of the analysis is given in Figure S2). This is in contrast to the strongly preferred orientation of hexagonal networks on G/SiC.[27,55] Hence, lack of a single preferred orientation in the present study would suggest the lack of strongly preferred angles between the BTB network and the underlying graphene lattice. The lack of alignment between the assembled molecular overlayer and weakly interacting graphene has been noted in some other studies[56,57] and is suggestive of an assembly dictated by molecule−molecule, rather than molecule−substrate, interactions.[6]

The structure of the assembled network as well as the constituent BTB molecules can be seen more clearly in the zoomed-in STM image shown in Figure 1c. The 3-fold symmetric BTB molecules appear as symmetric triangular spots at the vertices of the pore—the shape and size match those of the molecule lying flat on a surface. Each pore is surrounded by six such flat-lying molecules, with each molecule being shared by three adjacent rings. This assignment is strongly supported by the DFT calculations, showing very good agreement between simulated (given in Figure 1d) and experimental images. The calculations predict that the

DOI: 10.1021/acs.jpcc.6b01638
J. Phys. Chem. C 2016, 120, 8772−8780

molecules in the network are not completely flat on the graphene substrate, with the phenyl groups rotated by angles in the range of about 3°−10°. The assembly of the network is facilitated by the formation of two symmetric hydrogen bonds (O−H···O) between the terminal carboxylic groups of adjacent molecules. In this way, all three carboxylic groups of an individual molecule participate in the energetically favorable linear hydrogen bonding, explaining the excellent stability of the network. In fact, according to the DFT calculations, two molecules on graphene have a binding energy gain upon forming the hydrogen bonds of 1.4 eV (per pair of symmetric hydrogen bonds), and this reduces slightly to 1.3 eV in the more constrained network. The arrangement of stabilization by hydrogen bonds is further illustrated by the atomistic model of the BTB network on graphene shown in Figure 1e.

While the simulation considers BTB assembly on a flat graphene layer, the experiments have been carried out on epitaxial G/Ir(111), which exhibits a well-known moiré pattern due to the lattice mismatch between graphene and the Ir(111) substrate.[58,59] The contrast in Figure 1c has been enhanced to show the hexagonal superstructure formed by graphene on Ir(111) (moiré unit cell indicated), in the left side of the image. With a periodicity of ∼2.5 nm, closely matching the pore size of the overlaying BTB network, the moiré pattern might guide the BTB assembly process. However, our observations indicate that the BTB assembly is not affected by the moiré pattern. As seen in Figure 1c, the symmetry axes of the BTB network and the graphene moiré are not aligned. Furthermore, the angles between the neighboring BTB domains on the same G/Ir(111) terrace (i.e., uniform moiré pattern) have a broad distribution (Figure S2). These complementary observations indicate the lack of a single preferred orientation between the BTB network and the moiré. Additionally, we do not observe the signatures of molecular assembly strongly influenced by graphene moiré, viz., preferential adsorption at valley sites[60,61] and preferred angle of adsorption.[62] It is worth noting that these observations were made on epitaxial graphene on ruthenium or rhodium where the graphene moiré is highly corrugated (corrugation amplitude >1 Å), and the local work function of the surface varies strongly over the moiré unit cell.[7] Graphene on iridium is weakly corrugated (<0.5 Å), and the moiré is in general not expected to guide the assembly.

We observe two different typical grain boundaries between domains of the hexagonal network. The domains which are rotated with respect to each other resolve through the formation of pentamer−heptamer cavities (Figure 2a). The structures closely resemble those predicted and observed for graphene grain boundaries[63,64] and in TMA molecular networks on Au(111).[31] Conversely, the domain boundary structure shown in Figure 2b forms between laterally displaced hexagonal domains, in a fashion similar to that reported for self-assembly of TMA on Au(111) in UHV.[31] In some regions a continuous domain of the hexagonal network is found to have a series of misaligned rows with embedded topological defects (Figure S2)—some of these defects are identical to dislocations discussed in relation to topological defects in polycrystalline graphene.[63] The realignment of the rows again indicates the highly flexible nature of the network.

By controlling the BTB coverage and by annealing the sample, we can exclusively form the honeycomb phase of the BTB assembly. Increasing the coverage or lower annealing temperature results in other structures, as illustrated in Figure 2c−e. On room temperature deposition of 0.2 ML of BTB the

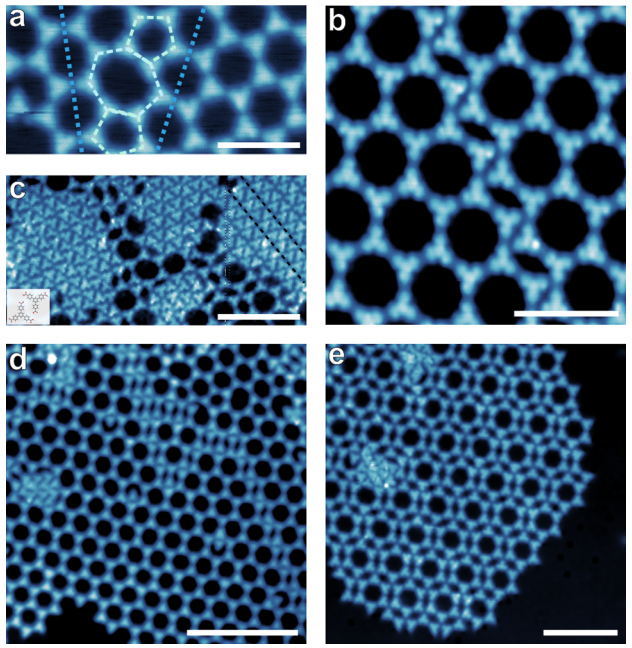

Figure 2. (a) Typical boundary structures between misaligned domains. Set-point parameters 1.84 V/20 pA. Scale bar 5 nm. (b) Domain wall structure between domains with the same orientation. Set-point parameters 1.64 V/15 pA. Scale bar 5 nm. Images in panels a and b are taken from a sample annealed at 373 K. (c) Close-packed phase in BTB assembly before annealing. The inset shows the constituting BTB dimer motif while a close-packed ribbon phase is indicated near the top-right corner. Set-point parameters 1.68 V/8.1 pA. Scale bar 10 nm. (d) Large scale image of BTB assembly at lower coverage without annealing. Set-point parameters 1.73 V/9.9 pA. Scale bar 15 nm. (e) Example of a BTB flower structure obtained after annealing a sample with low BTB coverage at 340 K. Set-point parameters 1.78 V/13 pA. Scale bar 10 nm.

hexagonal network is often found to be interspaced with close-packed islands (Figure 2c). Closer inspection reveals that these islands are characterized by a BTB dimer motif consisting of two tightly packed molecules, as indicated in the inset of Figure 2c. While mostly randomly oriented, sometimes these dimers are seen to organize in a 1D ribbon structure (indicated near the top-right corner of Figure 2c) with a periodicity of ∼1.6 nm along a row; the inter-row distance is ∼2.2 nm. The structure obtained after deposition of 0.1 ML of BTB on the substrate kept at room temperature (Figure 2d), although dominated by small domains of the honeycomb network, is frequently interrupted by pentamer−heptamer and dislocation cavities and close-packed islands. Point defects in the form of missing BTB molecules in the network or extra molecules in the pores of the network are also observed regularly. Annealing the sample at 340 K for an hour improves the long-range order of the assembly with a marked increase in the domain size of the hexagonal network, along with a reduction in the number of point defects and amount of other phases. Occasionally, we also observe another phase of growth, the flower structure, with a similar hexagonal pore size, but increased pore-to-pore distance of ∼5 nm. An isolated island of the flower structure is shown in Figure 2e. Finally, annealing the sample at 373 K for an hour leads to the exclusive formation of extended domains of the hexagonal porous network as shown in Figure 1a. These observations are in stark contrast to those reported for the effect of annealing on the assembly of BTB on Ag(111).[33]

DOI: 10.1021/acs.jpcc.6b01638
J. Phys. Chem. C 2016, 120, 8772−8780

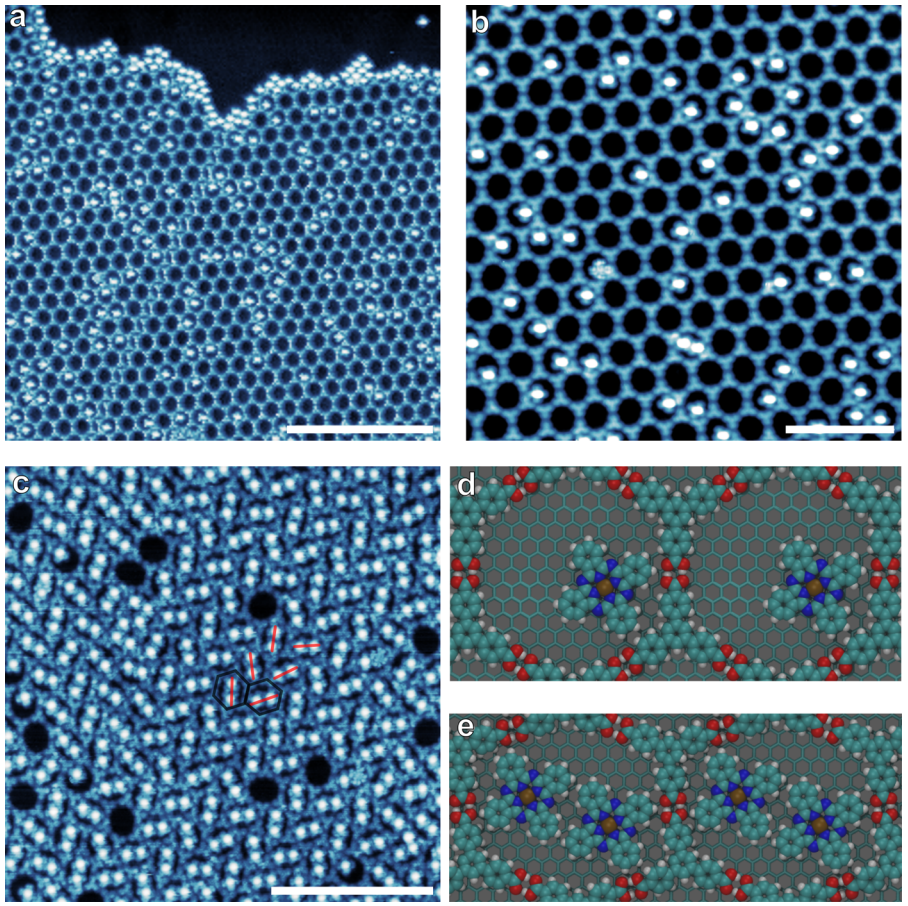

Figure 3. (a) Overview image of CoPC molecules in BTB network. Imaging parameters 1.49 V/3.6 pA. Scale bar 25 nm. (b) Zoomed-in image in the low CoPC coverage regime. Set-point parameters 1.49 V/3.1 pA. Scale bar 10 nm. (c) STM image at high CoPC coverage; the red lines highlight the arms of the herringbone pattern formed by CoPCs in the BTB network. Set-point 1.41 V/7.1 pA. Scale bar 15 nm. Deposition of CoPC was done with the BTB/G/Ir sample at room temperature; no further tempering was performed. (d) Atomistic model showing preference of CoPC molecules for the H-bonding site in BTB pore under single occupancy. (e) Atomistic model of 2 CoPCs in elongated BTB pores.

There, heating was seen to drive the assembly from the open chicken-wire phase to a denser porous phase to a closely packed compact phase. It is worth noting that the last two phases were associated with deprotonation of the BTB molecule on the metallic surface, resulting in increased molecule−substrate interaction. On graphene, the molecule−molecule interactions dominate, and heating only makes the molecules more mobile. This facilitates the assembly of the more porous hexagonal network which maximizes the energetically favorable linear H-bonds in the assembly. Two phases commonly found in previous studies of assembly of BTB—the porous oblique phase[34,36] and the compact phase[33,36]—were not seen in the present study.

One of the appealing aspects of molecular networks is their tunability. We demonstrate this by repeating the network formation with TMA molecules. They have the same binding motif as BTB but result in a network with a shorter period (shown in Figure S3). While we can grow honeycomb domains with ∼100 nm size, we were not able to achieve similar uniformity compared with BTB networks; multiple phases of growth are observed even after an annealing step. Therefore, we focus on the honeycomb BTB network to host suitable guest molecules. The well-studied π-conjugated molecule CoPC, which assembles into a compact square lattice on UHV deposition onto G/Ir(111),[65,66] is chosen for this purpose.

Figure 3a shows the result of deposition of 0.1 ML of CoPC on the G/Ir(111) substrate with the BTB network. The deposition was done with the sample at room temperature. Prior to the deposition of CoPC, the BTB/G/Ir sample was annealed at 373 K for an hour to form the extended honeycomb networks. Notably, for all coverages of CoPC discussed here, no annealing was done after deposition of the molecules. In the image, the CoPC molecules are seen as bright protrusions, either occupying the cavities of the BTB network in a random fashion or assembling at the edge of the network in a square lattice. Significantly no molecules are observed on top of the BTB molecules or even in the smaller cavities formed between the laterally displaced domains of BTB hexagonal network. The CoPC−graphene interaction is dominated by van der Waals interactions; i.e., the molecule is physisorbed on graphene. On the basis of orbital imaging and DFT calculations (see below), we do not expect strong interactions (e.g., due to hybridization) between the CoPC and graphene.

The CoPC molecules lie flat on the surface and do not occupy the center of the pore as can be seen in the smaller scale image given in Figure 3b. In fact, the lobes of the guest CoPC molecule display a marked preference for the H-bonding site between two BTB molecules, with two adjacent lobes of a CoPC molecule lying close to two adjacent H-bonding sites of the BTB network. Simulations show that there is an increase in adsorption energy of about 0.2 eV when CoPC is at the edge of

DOI: 10.1021/acs.jpcc.6b01638
J. Phys. Chem. C 2016, 120, 8772−8780

the pore, binding close to the COOH groups (see Figure 3d). Within this restriction, however, the guest molecules are seen to be arranged randomly across all six possible adsorption sites in a pore. Even in this low molecular coverage regime, occasional pores are seen to have two CoPC molecules in them. The guest molecules are observed to align themselves along the diagonal of the pore. In all cases the isolated CoPC molecules could be imaged with ease—this implies that the CoPC molecules are stabilized by the network, preventing them from being manipulated by the STM tip while scanning.[42,67]

The observation of two molecules in a single pore is surprising as the pore diameter is slightly too small to accommodate two CoPC molecules. However, due to the flexibility of the BTB network, CoPC dimer adsorption is associated with a slight elongation of the pore along the diagonal. This is mirrored by the DFT calculations: they predict that it is unfavorable to adsorb two molecules in an undistorted pore (adsorption energy of 3.0 eV per molecule in a pair compared to 3.5 eV for a single molecule). However, the pores are soft, and elongating them slightly is not energetically too unfavorable. Reproducing the slight elongation of the pore seen in experiments, the difference in the adsorption energies per CoPC molecule in a singly or double occupied BTB pore reduces to less than 0.1 eV and both configurations are probable.

Further deposition of CoPC on the same substrate again leads to a random distribution of the guest molecules in the pores of the host network. The numbers of empty pores and pores with one or two CoPC are consistent with random filling of the pores with CoPC (Figure S4). No more than two CoPC molecules are seen in the pores. Finally, after the deposition of about 0.8 ML of CoPC the pores are mostly doubly occupied, as can be seen in Figure 3c. Closer inspection of the image reveals a periodic arrangement of the guest molecules. As indicated in the figure, they form a herringbone arrangement with each arm of the pattern consisting of two CoPC molecules in a pore. The angle between the arms is slightly less than 90°, while the perpendicular distance between a parallel pair of molecules is ∼3.2 nm. The elongation direction of the pores can be visualized in the occasional vacant pores. Some of the vacant pores are more elongated than the others, indicating a relaxation of the network at these sites. Notably, although elongated, the network does not suffer from a complete distortion due to incorporation of the guest molecules, as reported in host structures stabilized by van der Waals forces[41,68]—the stronger hydrogen bonds between the BTB molecules accommodate the stretching without being broken.

Capturing the herringbone pattern in a DFT calculation would require using a much larger simulation cell, which renders this approach impractical. Instead, we have constructed a very simple model of the flexible network. The molecules are simulated by two-dimensional rigid bodies (no overlap allowed) with translational and rotational degrees of freedom on the simulation plane. The H-bonds between neighboring BTB molecules are simulated by two harmonic springs, and the energy of the system is calculated as the sum of the elastic potential energy of these springs. Further details can be found in the Methods section and the Supporting Information. Using this classical toy model of the BTB hexagonal lattice, we can easily estimate the energy of a large network stretched by CoPC molecules. We start by considering a small subset of pores and carefully place two CoPC inside each one, so that the pores are stretched along the same axis (Figure 4a). The resulting lattice stretching energy is about 9.7 au (arbitrary units), and the structure appears to be stable. However, upon annealing it undergoes a phase transition, and the herringbone pattern appears (Figure 4b). After cooling the system, the energy is lowered to about 8.4 au, indicating that the new structure is preferred. This simple calculation demonstrates that the herringbone pattern formation can be driven by the reduction of the elastic energy of the BTB network. The herringbone pattern minimizes the energy cost associated with stretching and twisting the hydrogen bonds between the BTB molecules.

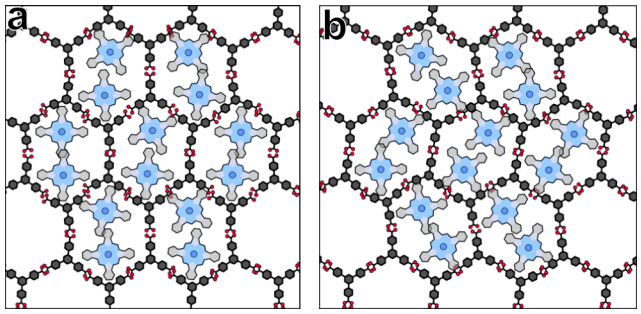

Figure 4. (a) Toy-model starting configuration, with seven doubly occupied pores aligned along the vertical direction, and (b) the one obtained after annealing and cooling.

Having investigated the structure of the BTB network and its application as a template for deposition of CoPC, we probe the electronic properties of the network and its electronic effects on the guest molecules using STM and STS. The spectra obtained on different regions of the empty BTB network on G/Ir(111) are shown in Figure 5a. These spectra are taken at a constant current (i.e., the bias is changed while keeping the tunneling current constant) to maximize the dI/dV signal while limiting the current to maintain stable tip−BTB−substrate junction. The spectrum obtained on graphene in the pore is found to be similar to bare graphene and is featureless. The one obtained at the center of the BTB molecule show two peaks at 2.1 and 2.8 V and can be interpreted as resonances originating from the lowest unoccupied molecular orbital (LUMO) and the LUMO +1, respectively. The highest occupied molecular orbital (HOMO) of the molecule, corresponding to a peak in the spectra at negative bias, is not observed at biases down to −3 V. DFT calculations predict energies of −2.0, 1.2, and 1.8 V for HOMO, LUMO, and LUMO+1, respectively (Figure S5). This difference between the observed and simulated orbital energies stems from the fact that measured values correspond to temporary charging of the molecule. That is, the peaks in the experimental dI/dV spectra correspond to the positive and negative ion resonances, and the energies differ from the calculated single-particle energy levels by the charging energy.[69,70]

The spatial dependence of the molecular orbitals can be probed by recording the spatially resolved dI/dV signal at the aforementioned voltages. These maps in the constant-height mode are shown in Figure 5b. The in-gap map at 1.2 V is akin to the topographical image, and contrast over the molecule corresponds to the modification of the tunneling barrier height due to the molecules. In the map taken at energy corresponding to the LUMO (2.1 V), the contrast is localized around the benzene rings, and the backbone is visible as darker region in between. The contrast gets further accentuated in the map at LUMO+1 (2.8 V). In all three maps, no special features are

DOI: 10.1021/acs.jpcc.6b01638
J. Phys. Chem. C 2016, 120, 8772−8780

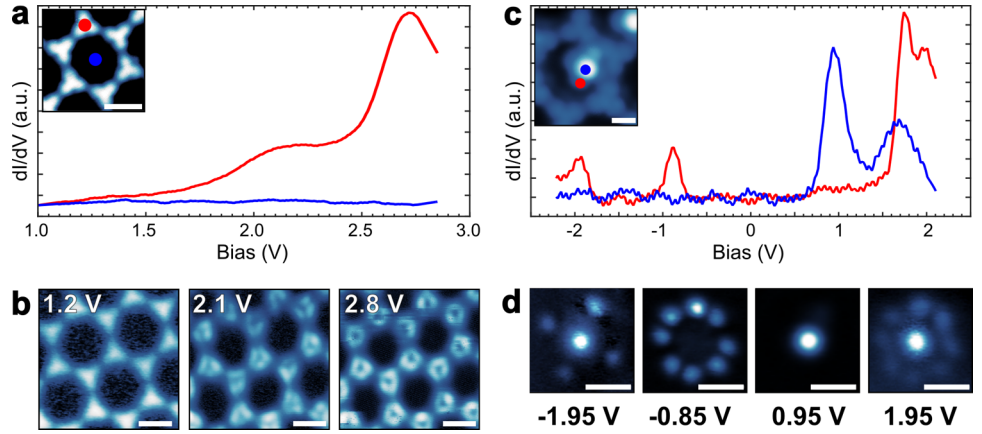

Figure 5. (a) Constant-current spectra measured on the BTB network on G/Ir(111). Positions of the spectra are indicated in the inset. (b) Constant-height dI/dV maps of the BTB network at the indicated bias voltages. Scale bar for all images is 2 nm. (c) Constant-height dI/dV spectra on the CoPC molecule adsorbed in a pore of the BTB network. Positions of the spectra are indicated in the inset. (d) Constant-height dI/dV maps of the CoPC molecule at the indicated bias voltages corresponding to (from left to right) HOMO−1, HOMO, LUMO, and LUMO+1. Scale bar for all images is 1 nm.

seen on the graphene region enclosed by the pores. These maps are reasonably well-reproduced by the DFT results (Figure S5) with no features in the graphene region.

Trapping a CoPC molecule in the pore of a BTB network is a convenient means of doing spectroscopy on a single molecule, as room-temperature deposition on G/Ir(111) usually results in close-packed assemblies. In addition, it serves to mechanically stabilize the molecules, in contrast to individual molecules on graphene that require exceedingly small set-point currents to be used for stable imaging and spectroscopy. The spectra taken (with the feedback loop open) on a CoPC molecule trapped in a pore, seen in Figure 5c, bear remarkable similarity to those obtained on molecules on bare graphene and h-BN.[66,71,72] Spectra on the central metal core show peak corresponding to LUMO and LUMO+1 at 0.94 and 1.68 V, respectively, whereas those on the organic lobes show peaks corresponding to HOMO−1, HOMO, and LUMO+1 at −1.93, −0.87, and 1.69 V, respectively. The positions of the peaks show some variation across the network. The variation has a similar magnitude as in close-packed CoPC on G/Ir(111).[66] Therefore, we conclude that the variation is due to a slight gating of the resonances due to adsorption at different sites of the moiré and not due to the presence of the BTB network. Importantly, no major variation in either the position or the line width of the peaks is observed for CoPC molecules lying at different orientation in the pores or in those in doubly occupied pores. Constant-height dI/dV maps of a CoPC molecule in a pore at voltages corresponding to the resonances are shown in Figure 5d. They are similar to the shape of an isolated CoPC molecule on h-BN.[72] The spectra and the maps prove that the network does not affect the electronic properties of the guest molecule and only serve to stabilize them mechanically.

CONCLUSIONS

In summary, we have demonstrated large-scale, high-quality honeycomb networks of BTB on a graphene model surface. The networks can be used as soft, flexible templates to pattern the adsorption of guest molecules. In addition to potential applications in templating, e.g., dopant molecules in graphene devices or spatially arranging catalytically active molecules on graphene, the networks can be used to isolate individual molecules on "slippy" surfaces, which is important for a range of high-resolution spectroscopic studies of molecule−graphene interactions.

Deposition of more than one CoPC molecule per pore causes a reorganization of the template to minimize the elastic energy stored in the hydrogen bonds of the BTB network. This causes the guest CoPC dimers to form a herringbone pattern, showing how the template symmetry can be broken in these soft, flexible templates to accommodate the guest molecules. This phenomenon is expected to be general and to occur on flexible networks on weakly interacting substrates. In addition to the general interest in formation of host−guest networks with a controlled packing and symmetry, the adsorption of two molecules per pore could be used to build controlled heterodimers on graphene. This would allow the study intermolecular interactions in dimers on graphene, including for example charge transfer and magnetic interactions.

ASSOCIATED CONTENT

Supporting Information

The Supporting Information is available free of charge on the ACS Publications website at DOI: 10.1021/acs.jpcc.6b01638.

STM images of BTB network growing uninterrupted over wrinkles and step edges; line profile over BTB network; statistics on misoriented BTB domains; STM image of topological defect in a BTB domain; STM images and description of self-assembled TMA network on G/Ir; STM image of 0.25 ML of CoPC in BTB network; simulated and experimental values of pore occupancy of BTB network under varying coverage of CoPC; simulated LDOS maps of BTB network at LUMO and LUMO+1; calculated DOS of BTB network; schematic diagram of toy model (PDF)

AUTHOR INFORMATION

Corresponding Author

*E-mail peter.liljeroth@aalto.fi (P.L.).

Author Contributions

K.B. and A.K. contributed equally to this work.

Notes

The authors declare no competing financial interest.

DOI: 10.1021/acs.jpcc.6b01638
J. Phys. Chem. C 2016, 120, 8772−8780

■ ACKNOWLEDGMENTS

This research made use of the Aalto Nanomicroscopy Center (Aalto NMC) facilities and was supported by the European Research Council (ERC-2011-StG No. 278698 "PRECISE-NANO"), the Academy of Finland through its Centres of Excellence Program (projects no. 284594 and 284621), and EU project PAMS (contract no. 610446). We acknowledge the computational resources provided by Aalto Science-IT project and Finland's IT Center for Science (CSC).

■ REFERENCES

(1) Rosei, F.; Schunack, M.; Naitoh, Y.; Jiang, P.; Gourdon, A.; Laegsgaard, E.; Stensgaard, I.; Joachim, C.; Besenbacher, F. Properties of Large Organic Molecules on Metal Surfaces. *Prog. Surf. Sci.* **2003**, *71*, 95−146.

(2) Otero, R.; Gallego, J. M.; Vázquez de Parga, A. L.; Martín, N.; Miranda, R. Molecular Self-Assembly at Solid Surfaces. *Adv. Mater.* **2011**, *23*, 5148−5176.

(3) Mao, H. Y.; Lu, Y. H.; Lin, J. D.; Zhong, S.; Wee, A. T. S.; Chen, W. Manipulating the Electronic and Chemical Properties of Graphene Via Molecular Functionalization. *Prog. Surf. Sci.* **2013**, *88*, 132−159.

(4) Kong, L.; Enders, A.; Rahman, T. S.; Dowben, P. A. Molecular Adsorption on Graphene. *J. Phys.: Condens. Matter* **2014**, *26*, 443001.

(5) Cai, B.; Zhang, S.; Yan, Z.; Zeng, H. Noncovalent Molecular Doping of Two-Dimensional Materials. *ChemNanoMat* **2015**, *1*, 542−557.

(6) MacLeod, J. M.; Rosei, F. Molecular Self-Assembly on Graphene. *Small* **2014**, *10*, 1038−1049.

(7) Batzill, M. The Surface Science of Graphene: Metal Interfaces, CVD Synthesis, Nanoribbons, Chemical Modifications, and Defects. *Surf. Sci. Rep.* **2012**, *67*, 83−115.

(8) Wintterlin, J.; Bocquet, M.-L. Graphene on Metal Surfaces. *Surf. Sci.* **2009**, *603*, 1841−1852.

(9) Mali, K. S.; Greenwood, J.; Adisoejoso, J.; Phillipson, R.; De Feyter, S. Nanostructuring Graphene for Controlled and Reproducible Functionalization. *Nanoscale* **2015**, *7*, 1566−1585.

(10) Georgakilas, V.; Otyepka, M.; Bourlinos, A. B.; Chandra, V.; Kim, N.; Kemp, K. C.; Hobza, P.; Zboril, R.; Kim, K. S. Functionalization of Graphene: Covalent and Non-Covalent Approaches, Derivatives and Applications. *Chem. Rev.* **2012**, *112*, 6156−6214.

(11) Dai, L. Functionalization of Graphene for Efficient Energy Conversion and Storage. *Acc. Chem. Res.* **2013**, *46*, 31−42.

(12) Li, B.; Klekachev, A. V.; Cantoro, M.; Huyghebaert, C.; Stesmans, A.; Asselberghs, I.; De Gendt, S.; De Feyter, S. Toward Tunable Doping in Graphene FETs by Molecular Self-Assembled Monolayers. *Nanoscale* **2013**, *5*, 9640−9644.

(13) Choudhury, D.; Das, B.; Sarma, D. D.; Rao, C. N. R. XPS Evidence for Molecular Charge-Transfer Doping of Graphene. *Chem. Phys. Lett.* **2010**, *497*, 66−69.

(14) Sun, J. T.; Lu, Y. H.; Chen, W.; Feng, Y. P.; Wee, A. T. S. Linear Tuning of Charge Carriers in Graphene by Organic Molecules and Charge-Transfer Complexes. *Phys. Rev. B: Condens. Matter Mater. Phys.* **2010**, *81*, 155403.

(15) Wang, X.; Xu, J.-B.; Xie, W.; Du, J. Quantitative Analysis of Graphene Doping by Organic Molecular Charge Transfer. *J. Phys. Chem. C* **2011**, *115*, 7596−7602.

(16) Park, C.-H.; Yang, L.; Son, Y.-W.; Cohen, M. L.; Louie, S. G. Anisotropic Behaviours of Massless Dirac Fermions in Graphene Under Periodic Potentials. *Nat. Phys.* **2008**, *4*, 213−217.

(17) Park, C.-H.; Yang, L.; Son, Y.-W.; Cohen, M. L.; Louie, S. G. New Generation of Massless Dirac Fermions in Graphene Under External Periodic Potentials. *Phys. Rev. Lett.* **2008**, *101*, 126804.

(18) Hunt, B.; Sanchez-Yamagishi, J. D.; Young, A. F.; Yankowitz, M.; LeRoy, B. J.; Watanabe, K.; Taniguchi, T.; Moon, P.; Koshino, M.; Jarillo-Herrero, P.; et al. Massive Dirac Fermions and Hofstadter Butterfly in a van der Waals Heterostructure. *Science* **2013**, *340*, 1427−1430.

(19) Yankowitz, M.; Xue, J.; Cormode, D.; Sanchez-Yamagishi, J. D.; Watanabe, K.; Taniguchi, T.; Jarillo-Herrero, P.; Jacquod, P.; LeRoy, B. J. Emergence of Superlattice Dirac Points in Graphene on Hexagonal Boron Nitride. *Nat. Phys.* **2012**, *8*, 382−386.

(20) Song, Y.; Luo, Y.; Zhu, C.; Li, H.; Du, D.; Lin, Y. Recent Advances in Electrochemical Biosensors Based on Graphene Two-Dimensional Nanomaterials. *Biosens. Bioelectron.* **2016**, *76*, 195−212.

(21) Wu, S.; He, Q.; Tan, C.; Wang, Y.; Zhang, H. Graphene-Based Electrochemical Sensors. *Small* **2013**, *9*, 1160−1172.

(22) Zhang, N.; Zhang, Y.; Xu, Y.-J. Recent Progress on Graphene-Based Photocatalysts: Current Status and Future Perspectives. *Nanoscale* **2012**, *4*, 5792−5813.

(23) Barth, J. V. Fresh Perspectives for Surface Coordination Chemistry. *Surf. Sci.* **2009**, *603*, 1533−1541.

(24) Kudernac, T.; Lei, S.; Elemans, J. A.; De Feyter, S. Two-Dimensional Supramolecular Self-Assembly: Nanoporous Networks on Surfaces. *Chem. Soc. Rev.* **2009**, *38*, 402−421.

(25) Lackinger, M.; Heckl, W. M. Carboxylic Acids: Versatile Building Blocks and Mediators for Two-Dimensional Supramolecular Self-Assembly. *Langmuir* **2009**, *25*, 11307−11321.

(26) Theobald, J. A.; Oxtoby, N. S.; Phillips, M. A.; Champness, N. R.; Beton, P. H. Controlling Molecular Deposition and Layer Structure with Supramolecular Surface Assemblies. *Nature* **2003**, *424*, 1029−1031.

(27) Karmel, H. J.; Chien, T.; Demers-Carpentier, V.; Garramone, J. J.; Hersam, M. C. Self-Assembled Two-Dimensional Heteromolecular Nanoporous Molecular Arrays on Epitaxial Graphene. *J. Phys. Chem. Lett.* **2013**, *5*, 270−274.

(28) Dmitriev, A.; Lin, N.; Weckesser, J.; Barth, J. V.; Kern, K. Supramolecular Assemblies of Trimesic Acid on a Cu(100) Surface. *J. Phys. Chem. B* **2002**, *106*, 6907−6912.

(29) Lackinger, M.; Griessl, S.; Heckl, W. M.; Hietschold, M.; Flynn, G. W. Self-Assembly of Trimesic Acid at the Liquid-Solid Interface - a Study of Solvent-Induced Polymorphism. *Langmuir* **2005**, *21*, 4984−4988.

(30) Ye, Y.; Sun, W.; Wang, Y.; Shao, X.; Xu, X.; Cheng, F.; Li, J.; Wu, K. A Unified Model: Self-Assembly of Trimesic Acid on Gold. *J. Phys. Chem. C* **2007**, *111*, 10138−10141.

(31) Iancu, V.; Braun, K.-F.; Schouteden, K.; Van Haesendonck, C. Probing the Electronic Properties of Trimesic Acid Nanoporous Networks on Au(111). *Langmuir* **2013**, *29*, 11593−11599.

(32) Baviloliaei, M. S.; Diekhöner, L. Molecular Self-Assembly at Nanometer Scale Modulated Surfaces: Trimesic Acid on Ag(111), Cu(111) and Ag/Cu(111). *Phys. Chem. Chem. Phys.* **2014**, *16*, 11265−11269.

(33) Ruben, M.; Payer, D.; Landa, A.; Comisso, A.; Gattinoni, C.; Lin, N.; Collin, J.-P.; Sauvage, J.-P.; De Vita, A.; Kern, K. 2D Supramolecular Assemblies of Benzene-1,3,5-Triyl-Tribenzoic Acid: Temperature-Induced Phase Transformations and Hierarchical Organization with Macrocyclic Molecules. *J. Am. Chem. Soc.* **2006**, *128*, 15644−15651.

(34) Kampschulte, L.; Lackinger, M.; Maier, A.-K.; Kishore, R. S. K.; Griessl, S.; Schmittel, M.; Heckl, W. M. Solvent Induced Polymorphism in Supramolecular 1, 3, 5-Benzenetribenzoic Acid Monolayers. *J. Phys. Chem. B* **2006**, *110*, 10829−10836.

(35) Gutzler, R.; Sirtl, T.; Dienstmaier, J. F.; Mahata, K.; Heckl, W. M.; Schmittel, M.; Lackinger, M. Reversible Phase Transitions in Self-Assembled Monolayers at the Liquid- Solid Interface: Temperature-Controlled Opening and Closing of Nanopores. *J. Am. Chem. Soc.* **2010**, *132*, 5084−5090.

(36) Silly, F. Two-Dimensional 1,3,5-Tris(4-Carboxyphenyl) Benzene Self-Assembly at the 1-Phenyloctane/graphite Interface Revisited. *J. Phys. Chem. C* **2012**, *116*, 10029−10032.

(37) Cometto, F. P.; Kern, K.; Lingenfelder, M. Local Conformational Switching of Supramolecular Networks at the Solid/liquid Interface. *ACS Nano* **2015**, *9*, 5544−5550.

DOI: 10.1021/acs.jpcc.6b01638
J. Phys. Chem. C 2016, 120, 8772−8780

(38) Zhou, Q.; Li, Y.; Li, Q.; Wang, Y.; Yang, Y.; Fang, Y.; Wang, C. Switchable Supramolecular Assemblies on Graphene. *Nanoscale* **2014**, *6*, 8387−8391.
(39) MacLeod, J. M.; Lipton-Duffin, J. A.; Cui, D.; De Feyter, S.; Rosei, F. Substrate Effects in the Supramolecular Assembly of 1,3,5-Benzene Tricarboxylic Acid on Graphite and Graphene. *Langmuir* **2015**, *31*, 7016−7024.
(40) Stepanow, S.; Lingenfelder, M.; Dmitriev, A.; Spillmann, H.; Delvigne, E.; Lin, N.; Deng, X.; Cai, C.; Barth, J. V.; Kern, K. Steering Molecular Organization and Host-Guest Interactions Using Two-Dimensional Nanoporous Coordination Systems. *Nat. Mater.* **2004**, *3*, 229−233.
(41) Lu, J.; Lei, S.-B.; Zeng, Q.-D.; Kang, S.-Z.; Wang, C.; Wan, L.-J.; Bai, C.-L. Template-Induced Inclusion Structures with Copper(II) Phthalocyanine and Coronene As Guests in Two-Dimensional Hydrogen-Bonded Host Networks. *J. Phys. Chem. B* **2004**, *108*, 5161−5165.
(42) Griessl, S. J. H.; Lackinger, M.; Jamitzky, F.; Markert, T.; Hietschold, M.; Heckl, W. M. Incorporation and Manipulation of Coronene in an Organic Template Structure. *Langmuir* **2004**, *20*, 9403−9407.
(43) Zhang, X.; Zeng, Q.; Wang, C. Molecular Templates and Nano-Reactors: Two-Dimensional Hydrogen Bonded Supramolecular Networks on Solid/Liquid Interfaces. *RSC Adv.* **2013**, *3*, 11351−11366.
(44) Liu, J.; Chen, T.; Deng, X.; Wang, D.; Pei, J.; Wan, L.-J. Chiral Hierarchical Molecular Nanostructures on Two-Dimensional Surface by Controllable Trinary Self-Assembly. *J. Am. Chem. Soc.* **2011**, *133*, 21010−21015.
(45) Zhang, X.; Shen, Y.; Wang, S.; Guo, Y.; Deng, K.; Wang, C.; Zeng, Q. One Plus Two: Supramolecular Coordination in a Nano-Reactor on Surface. *Sci. Rep.* **2012**, *2*, 742.
(46) Kong, X.-H.; Deng, K.; Yang, Y.-L.; Zeng, Q.-D.; Wang, C. H-Bond Switching Mediated Multiple Flexibility in Supramolecular Host-Guest Architectures. *J. Phys. Chem. C* **2007**, *111*, 17382−17387.
(47) Van Gastel, R.; N'Diaye, A. T.; Wall, D.; Coraux, J.; Busse, C.; Buckanie, N. M.; Zu Heringdorf, F.-J. M.; Von Hoegen, M. H.; Michely, T.; Poelsema, B. Selecting a Single Orientation for Millimeter Sized Graphene Sheets. *Appl. Phys. Lett.* **2009**, *95*, 121901.
(48) http://gwyddion.net/.
(49) Kresse, G.; Furthmuller, J. Efficiency of Ab-Initio Total Energy Calculations for Metals and Semiconductors Using a Plane-Wave Basis Set. *Comput. Mater. Sci.* **1996**, *6*, 15.
(50) Kresse, G. Efficient Iterative Schemes for Ab Initio Total-Energy Calculations Using a Plane-Wave Basis Set. *Phys. Rev. B: Condens. Matter Mater. Phys.* **1996**, *54*, 11169−11186.
(51) Klimeš, J.; Bowler, D. R.; Michaelides, A. Chemical Accuracy for the van der Waals Density Functional. *J. Phys.: Condens. Matter* **2010**, *22*, 022201.
(52) Klimeš, J.; Bowler, D. R.; Michaelides, A. Van der Waals Density Functionals Applied to Solids. *Phys. Rev. B: Condens. Matter Mater. Phys.* **2011**, *83*, 195131.
(53) Blöchl, P. E. Projector Augmented-Wave Method. *Phys. Rev. B: Condens. Matter Mater. Phys.* **1994**, *50*, 17953−17979.
(54) Hofer, W. A.; Foster, A. S.; Shluger, A. L. Theories of Scanning Probe Microscopes at the Atomic Scale. *Rev. Mod. Phys.* **2003**, *75*, 1287−1331.
(55) Li, B.; Tahara, K.; Adisoejoso, J.; Vanderlinden, W.; Mali, K. S.; De Gendt, S.; Tobe, Y.; De Feyter, S. Self-Assembled Air-Stable Supramolecular Porous Networks on Graphene. *ACS Nano* **2013**, *7*, 10764−10772.
(56) Wang, Q. H.; Hersam, M. C. Room-Temperature Molecular-Resolution Characterization of Self-Assembled Organic Monolayers on Epitaxial Graphene. *Nat. Chem.* **2009**, *1*, 206−211.
(57) Cho, J.; Smerdon, J.; Gao, L.; Süzer, O.; Guest, J. R.; Guisinger, N. P. Structural and Electronic Decoupling of C_{60} from Epitaxial Graphene on SiC. *Nano Lett.* **2012**, *12*, 3018−3024.
(58) N'Diaye, A. T.; Coraux, J.; Plasa, T. N.; Busse, C.; Michely, T. Structure of Epitaxial Graphene on Ir(111). *New J. Phys.* **2008**, *10*, 043033.
(59) Hämäläinen, S. K.; Boneschanscher, M. P.; Jacobse, P. H.; Swart, I.; Pussi, K.; Moritz, W.; Lahtinen, J.; Liljeroth, P.; Sainio, J. Structure and Local Variations of the Graphene Moiré on Ir(111). *Phys. Rev. B: Condens. Matter Mater. Phys.* **2013**, *88*, 201406.
(60) Mao, J.; Zhang, H.; Jiang, Y.; Pan, Y.; Gao, M.; Xiao, W.; Gao, H.-J. Tunability of Supramolecular Kagome Lattices of Magnetic Phthalocyanines Using Graphene-Based Moiré Patterns As Templates. *J. Am. Chem. Soc.* **2009**, *131*, 14136−14137.
(61) Pollard, A. J.; Perkins, E. W.; Smith, N. A.; Saywell, A.; Goretzki, G.; Phillips, A. G.; Argent, S. P.; Sachdev, H.; Müller, F.; Hüfner, S.; et al. Supramolecular Assemblies Formed on an Epitaxial Graphene Superstructure. *Angew. Chem., Int. Ed.* **2010**, *49*, 1794−1799.
(62) Zhang, H.; Sun, J.; Low, T.; Zhang, L.; Pan, Y.; Liu, Q.; Mao, J.; Zhou, H.; Guo, H.; Du, S.; et al. Assembly of Iron Phthalocyanine and Pentacene Molecules on a Graphene Monolayer Grown on Ru (0001). *Phys. Rev. B: Condens. Matter Mater. Phys.* **2011**, *84*, 245436.
(63) Yazyev, O. V.; Louie, S. G. Electronic Transport in Polycrystalline Graphene. *Nat. Mater.* **2010**, *9*, 806−809.
(64) Huang, P. Y.; Ruiz-Vargas, C. S.; van der Zande, A. M.; Whitney, W. S.; Levendorf, M. P.; Kevek, J. W.; Garg, S.; Alden, J. S.; Hustedt, C. J.; Zhu, Y.; et al. Grains and Grain Boundaries in Single-Layer Graphene Atomic Patchwork Quilts. *Nature* **2011**, *469*, 389−392.
(65) Hämäläinen, S. K.; Stepanova, M.; Drost, R.; Liljeroth, P.; Lahtinen, J.; Sainio, J. Self-Assembly of Cobalt-Phthalocyanine Molecules on Epitaxial Graphene on Ir(111). *J. Phys. Chem. C* **2012**, *116*, 20433−20437.
(66) Järvinen, P.; Hämäläinen, S. K.; Ijäs, M.; Harju, A.; Liljeroth, P. Self-Assembly and Orbital Imaging of Metal Phthalocyanines on a Graphene Model Surface. *J. Phys. Chem. C* **2014**, *118*, 13320−13325.
(67) Griessl, S. J. H.; Lackinger, M.; Jamitzky, F.; Markert, T.; Hietschold, M.; Heckl, W. M. Room-Temperature Scanning Tunneling Microscopy Manipulation of Single C_{60} Molecules at the Liquid-Solid Interface: Playing Nanosoccer. *J. Phys. Chem. B* **2004**, *108*, 11556−11560.
(68) Zhang, H.; Xiao, W. D.; Mao, J.; Zhou, H.; Li, G.; Zhang, Y.; Liu, L.; Du, S.; Gao, H.-J. Host-Guest Superstructures on Graphene-Based Kagome Lattice. *J. Phys. Chem. C* **2012**, *116*, 11091−11095.
(69) Repp, J.; Meyer, G.; Stojković, S. M.; Gourdon, A.; Joachim, C. Molecules on Insulating Films: Scanning-Tunneling Microscopy Imaging of Individual Molecular Orbitals. *Phys. Rev. Lett.* **2005**, *94*, 026803.
(70) Swart, I.; Gross, L.; Liljeroth, P. Single-Molecule Chemistry and Physics Explored by Low-Temperature Scanning Probe Microscopy. *Chem. Commun.* **2011**, *47*, 9011−9023.
(71) Schulz, F.; Drost, R.; Hämäläinen, S. K.; Liljeroth, P. Templated Self-Assembly and Local Doping of Molecules on Epitaxial Hexagonal Boron Nitride. *ACS Nano* **2013**, *7*, 11121−11128.
(72) Schulz, F.; Ijäs, M.; Drost, R.; Hämäläinen, S. K.; Harju, A.; Seitsonen, A. P.; Liljeroth, P. Many-Body Transitions in a Single Molecule Visualized by Scanning Tunnelling Microscopy. *Nat. Phys.* **2015**, *11*, 229−234.

DOI: 10.1021/acs.jpcc.6b01638
J. Phys. Chem. C 2016, 120, 8772−8780